# SUPPORTING INFORMATION

## Redox Potentials and Electronic States of Iron Porphyrin IX Adsorbed on Single Crystal Gold Electrode Surfaces

*Ling Zhang, Kasper P. Kepp, Jens Ulstrup,* Jingdong Zhang**

**Table S1.** The peak width of half height of anodic and cathodic peaks (V) and the peak separations ($\Delta E$, V) of the high−potential (-0.20 V vs. NHE) and low−potential (-0.42 V) peaks in cyclic voltammograms (CVs) of FePPIX adsorbed on Au(111) single−crystal electrode at pH 11.7 at different scan rates ($v$, V/s).

| $v$, V $s^{-1}$ | High−potential peaks (-0.20 V) | | | Low−potential peaks (-0.42 V) | | |
|---|---|---|---|---|---|---|
| | Anodic peak−width | Cathodic peak−width | $\Delta E$, V | Anodic peak width | Cathodic peak width | $\Delta E$, V |
| **0.2** | 0.101±0.006 | 0.098±0.003 | 0.022 | 0.091±0.009 | 0.085±0.008 | 0.014 |
| **0.3** | 0.101±0.002 | 0.095±0.002 | 0.022 | 0.090±0.022 | 0.090±0.013 | 0.0 |
| **0.4** | 0.111±0.004 | 0.102±0.004 | 0.014 | 0.099±0.014 | 0.092±0.010 | 0.002 |
| **0.5** | 0.108±0.004 | 0.106±0.006 | 0.022 | 0.099±0.015 | 0.095±0.004 | 0.0 |
| **0.7** | 0.114±0.008 | 0.110±0.002 | 0.015 | 0.100±0.007 | 0.089±0.005 | 0.0 |
| **1.0** | 0.121±0.015 | 0.113±0.003 | 0.017 | 0.100±0.007 | 0.095±0.005 | 0.015 |

**Table S2.** The peak width of half height of anodic and cathodic peaks (V) and the peak separations ($\Delta E$, V) of FePPIX adsorbed on basal plane graphite (BPG), edge−plane graphite (EPG) and glassy carbon (GC) electrodes with the midpoint potential of -0.39, -0.39, and -0.40 V at pH 11.7 at different scan rates ($v$, V/s).

| | | **BPG** | |
|---|---|---|---|
| ***v*, V s$^{-1}$** | **Anodic peak width** | **Cathodic peak width** | **$\Delta E$, V** |
| **0.2** | 0.093±0.009 | 0.091±0.009 | 0.037 |
| **0.3** | 0.094±0.009 | 0.095±0.010 | 0.024 |
| **0.4** | 0.129±0.013 | 0.124±0.012 | 0.0 |
| **0.5** | 0.138±0.014 | 0.134±0.013 | 0.025 |
| **0.7** | 0.135±0.014 | 0.135±0.014 | 0.026 |
| **1.0** | 0.141±0.014 | 0.126±0.013 | 0.0 |
| | | **EPG** | |
| ***v*, V s$^{-1}$** | **Anodic peak width** | **Cathodic peak width** | **$\Delta E$, V** |
| **0.2** | 0.125±0.013 | 0.106±0.011 | 0.014 |
| **0.3** | 0.138±0.014 | 0.123±0.012 | 0.032 |
| **0.4** | 0.150±0.015 | 0.141±0.014 | 0.032 |
| **0.5** | 0.156±0.016 | 0.136±0.014 | 0.024 |
| **0.7** | 0.164±0.016 | 0.140±0.014 | 0.034 |
| **1.0** | 0.153±0.015 | 0.139±0.014 | 0.056 |
| | | **GCE** | |
| ***v*, V s$^{-1}$** | **Anodic peak width** | **Cathodic peak width** | **$\Delta E$, V** |
| **0.2** | 0.125±0.016 | 0.126±0.016 | 0.015 |
| **0.3** | 0.128±0.011 | 0.128±0.011 | 0.022 |
| **0.4** | 0.129±0.010 | 0.129±0.010 | 0.027 |
| **0.5** | 0.130±0.012 | 0.130±0.012 | 0.039 |
| **0.7** | 0.134±0.010 | 0.134±0.010 | 0.049 |
| **1.0** | 0.136±0.011 | 0.136±0.011 | 0.068 |

**Table S3**. Midpoint potentials ($E_{1/2}$, vs. NHE) of FePPIX reported in the literature at the different pH and the values calibrated to pH 11.7 according to the Nernst equation, $\Delta E$ (V) = -0.059$\Delta pH$.

| **pH[ref.]** | $E_{1/2}$, **V** | **Functional materials** | **Supporting electrode** | **State of FePPIX** | **Ion strength** | $E_{1/2}$ **at pH 11.7, V** |
|---|---|---|---|---|---|---|
| **7.0**[1] | -0.140 | / | 11-amino-1-undecanethiol modified gold electrode | Chemically bonded | 0.01 M, phosphate buffer | -0.420 |
| **7.4**[2] | -0.152 | Graphene oxide nanosheets | Glassy carbon electrode | Physically adsorbed | 0.1 M, phosphate buffer | -0.406 |
| **9.5**[3] | -0.280 | / | Highly oriented pyrolytic graphite electrode | Physically adsorbed | 0.1 M, $Na_2B_4O_7$ buffer | -0.410 |
| **12.0**[4] | -0.439 | | | | 0.2 M, $NaClO_4$ and NaOH buffer | -0.421 |
| **9.8**[4] | -0.299 | / | Pyrolytic graphite electrode | Physically adsorbed | 0.1 M $NaClO_4$, 0.1 M carbonate buffer | -0.411 |
| **7.0**[4] | -0.129 | | | | 0.1 M $NaClO_4$, 0.1 M phosphate buffer | -0.406 |

**Table S4.** The peak width of half height of anodic and cathodic peaks (V) and the peak separations ($\Delta E$, V) of the high−potential and low−potential peaks in cyclic voltammograms (CVs) of FePPIX adsorbed on Au(110) and Au(100) single−crystal electrodes at pH 11.7 at different scan rates ($v$, V/s).

| **Au(110)** | **High−potential peaks** | | | **Low−potential peaks** | | |
|---|---|---|---|---|---|---|
| $v$, V s$^{-1}$ | **Anodic peak width** | **Cathodic peak width** | $\Delta E$, V | **Anodic peak width** | **Cathodic peak width** | $\Delta E$, V |
| **0.2** | 0.127±0.022 | 0.145±0.031 | 0.001 | 0.085±0.033 | 0.101±0.045 | 0.034 |
| **0.4** | 0.187±0.031 | 0.183±0.005 | 0.002 | 0.010±0.023 | 0.105±0.013 | 0.010 |
| **0.5** | 0.191±0.004 | 0.190±0.002 | 0.005 | 0.093±0.010 | 0.092±0.011 | 0.070 |
| **0.7** | 0.185±0.013 | 0.184±0.002 | 0.012 | 0.099±0.015 | 0.101±0.020 | 0.040 |
| **1.0** | 0.202±0.003 | 0.203±0.003 | 0.015 | 0.107±0.018 | 0.105±0.021 | 0.010 |
| **Au(100)** | **High−potential peaks** | | | **Low−potential peaks** | | |
| $v$, V s$^{-1}$ | **Anodic peak width** | **Cathodic peak width** | $\Delta E$, V | **Anodic peak width** | **Cathodic peak width** | $\Delta E$, V |
| **0.2** | 0.102±0.003 | 0.089±0.011 | 0.020 | −* | −* | −* |
| **0.4** | 0.110±0.006 | 0.094±0.008 | 0.020 | 0.093±0.002 | 0.084±0.006 | 0.030 |
| **0.5** | 0.107±0.012 | 0.099±0.004 | 0.024 | 0.106±0.008 | 0.100±0.005 | 0.013 |
| **0.7** | 0.112±0.009 | 0.106±0.001 | 0.022 | 0.103±0.004 | 0.103±0.004 | 0.042 |
| **1.0** | 0.123±0.001 | 0.114±0.006 | 0.032 | 0.108±0.010 | 0.104±0.005 | 0.0 |
| **Au(poly)** | **High−potential peaks** | | | **Low−potential peaks** | | |
| $v$, V s$^{-1}$ | **Anodic peak width** | **Cathodic peak width** | $\Delta E$, V | **Anodic peak width** | **Cathodic peak width** | $\Delta E$, V |
| **0.2** | 0.163±0.016 | 0.142±0.014 | 0.032 | 0.120±0.012 | 0.105±0.011 | 0.037 |
| **0.4** | 0.202±0.010 | 0.184±0.010 | 0.034 | 0.162±0.016 | 0.109±0.009 | 0.022 |
| **0.5** | 0.192±0.008 | 0.174±0.008 | 0.039 | 0.141±0.012 | 0.106±0.007 | 0.012 |
| **0.7** | 0.193±0.010 | 0.178±0.009 | 0.044 | 0.138±0.010 | 0.108±0.008 | 0.012 |
| **1.0** | 0.194±0.010 | 0.194±0.010 | 0.022 | 0.138±0.010 | 0.108±0.009 | 0.019 |

*Peaks are too small that values can be determined.

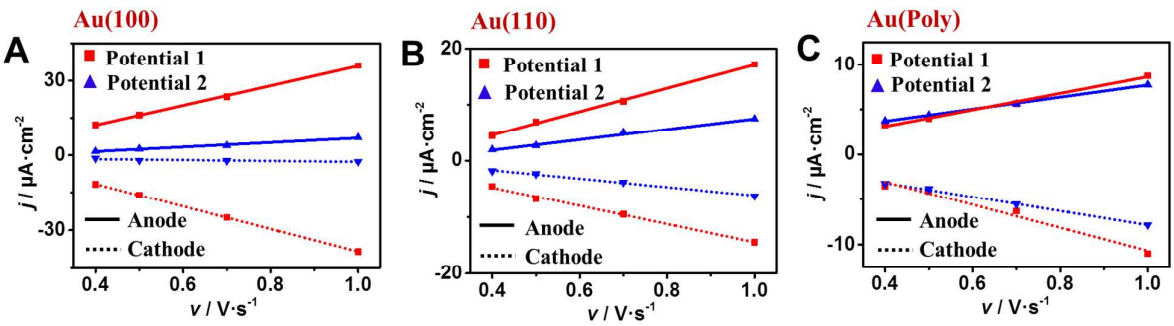


**Figure S1**. Anodic and cathodic peak current densities (j) versus scan rates (v) of FePPIX on Au(100) (A) , Au(110), and Au(poly) (D) electrodes. 10 μM FePPIX, 5 mM $NaClO_4$ pH 11.7.

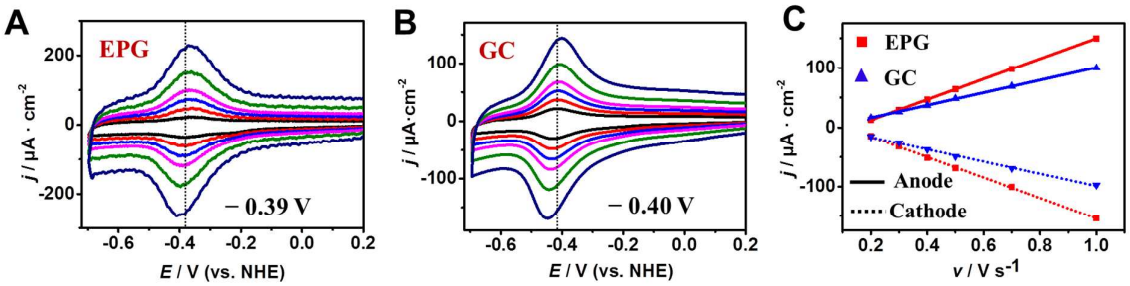


**Figure S2**. (A − C) CVs of EPG (A) and GC (B) electrodes in 10 μM hemin, 5 mM $NaClO_4$ pH 11.7 . Scan rates, 0.2, 0.3, 0.4, 0.5, 0.7, and 1.0 V $s^{-1}$. (C) Cathodic and anodic j−v plots for EPG and GC electrodes, respectively.

**Table S5. Electroactive Coverages of FePPIX Adsorbed on the Different Electrodes. 5 mM $NaClO_4$, pH 11.7.**

| Electrodes | $\Gamma$, mol $cm^{-2}$, and Ratio to Full Monolayer* | |
|---|---|---|
| | High−potential | Low−potential |
| Au(111) | $3.7(\pm 0.6) \times 10^{-11}$, 20% | $5.1(\pm 1.5) \times 10^{-12}$, 3.0% |
| Au(100) | $4.0(\pm 0.6) \times 10^{-11}$, 25% | $2.7(\pm 1.7) \times 10^{-12}$, 1.5% |
| Au(110) | $2.7(\pm 0.5) \times 10^{-11}$, 15% | $5.5(\pm 1.5) \times 10^{-12}$, 3.0% |
| Au(poly) | $1.3(\pm 0.2) \times 10^{-11}$, 7.6% | $8.7(\pm 0.2) \times 10^{-12}$, 5.1% |
| BPG | − | $1.8(\pm 0.8) \times 10^{-12}$, 100% |
| EPG | − | $2.0(\pm 0.5) \times 10^{-12}$, 100% |
| GC | − | $1.3(\pm 0.2) \times 10^{-10}$, 80% |

*Theoretical full monolayer, $1.7 \times 10^{-10}$ mol $cm^{-2}$ assuming closest packing of $1.0 \times 1.0$ $nm^2$ FePPIX molecules.

The Laviron equation[39], with a transfer coefficient $\alpha = 0.5$ and peak separation $\Delta E_p > 200$ mV was applied:

$$\Delta E_p = 4\frac{RT}{nF} ln \frac{1/2}{m} \qquad \text{(S1)}$$

$m$ is defined as $m = \frac{RTk_s}{Fnv}$, $F$ is Faraday's constant, 96485 A s mol$^{-1}$. $R$ the gas constant, 8.314 J K$^{-1}$ mol$^{-1}$, $n$ the number of electrons transferred (unity for the Fe(III)/(II) couple), $v$ the scan rate, V s$^{-1}$, and $k_s$ the electron transfer rate constant (s$^{-1}$).

By plotting $m^{-1}$ against $v$, $k_s$ is determined by the slope.

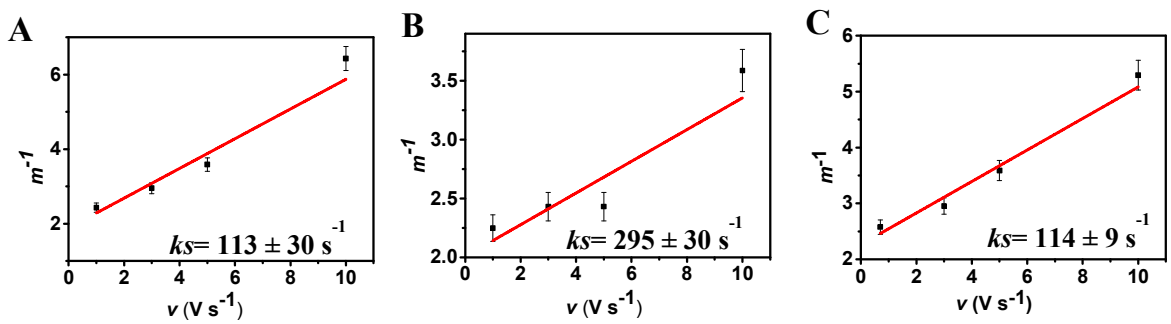


**Figure S3.** Calculations of $k_s$ (s$^{-1}$) for FePPIX adsorbed on Au(111) and BPG surfaces. Plots of $m^{-1}$ versus $v$ (V s$^{-1}$) for the high−potential peaks at -0.20 V (A) and low−potential peaks at -0.42 V (B) of FePPIX on Au(111), and -0.39 V on BPG (C).

**Table S6.** Computed DFT (TPSSh−D3/def2−TZVPP) energies of optimized penta−coordinated FePPIX models with distal $OH^-$ axial ligand, −Fe($OH^-$). HS = high−spin, LS = low−spin. The formal electrostatic charge on the iron center (*Q*), the single-point electronic ground state energies in units of hartree (*E/def2−TZVPP*), dispersion corrections in units of hartree (***D3 correction***), the high−spin/low−spin energy gap in KJ/mol ($\Delta E_{(HS\text{-}LS)}$) where a positive number signifies that low−spin is favored, and the vertical ionization energies and electron affinities ($\lambda$, hartree) used for computing reorganization energies ($\lambda$, KJ/mol).

| **Models** | **Oxidation and Spin states** | ***Q*** | ***E/def2-TZVPP*, hartree** | ***D3 correction*, hartree** | **$\Delta E_{(HS\text{-}LS)}$, kJ mol$^{-1}$** | **$\lambda$, hartree** | **$\lambda$, kJ mol$^{-1}$** |
|---|---|---|---|---|---|---|---|
| **Free** | HS Fe(III) | -2 | -3174.50629 | -0.07967 | 3.0 | -3174.62632 | 14.1 |
| | HS Fe(II) | -3 | -3174.62685 | -0.07948 | -30.3 | -3174.50146 | |
| | LS Fe(III) | -2 | -3174.50745 | -0.08105 | | -3174.61443 | |
| | LS Fe(II) | -3 | -3174.61533 | -0.08091 | | -3174.50391 | |
| **Au 7 atoms** | HS Fe(III) | -2 | -4124.69279 | -0.18670 | 70.9 | -4124.82142 | 54.1 |
| | HS Fe(II) | -3 | -4124.83305 | -0.18837 | 92.3 | -4124.70748 | |
| | LS Fe(III) | -2 | -4124.71980 | -0.19444 | | -4124.84827 | |
| | LS Fe(II) | -3 | -4124.86821 | -0.18455 | | -4124.71912 | |
| **carbon** | HS Fe(III) | -2 | -4250.52507 | -0.19260 | 37.0 | -4250.63701 | 64.8 |
| | HS Fe(II) | -3 | -4250.65351 | -0.19575 | -33.9 | -4250.52060 | |
| | LS Fe(III) | -2 | -4250.53917 | -0.19645 | | -4250.64742 | |
| | LS Fe(II) | -3 | -4250.64060 | -0.19514 | | -4250.53282 | |
| **Au 13 atoms** | HS Fe(III) | -2 | -4939.29410 | -0.25911 | 17.0 | -4939.43864 | 123.5 |
| | HS Fe(II) | -3 | -4939.37872 | -0.26183 | 129.7 | -4939.19477 | |
| | LS Fe(III) | -2 | -4939.30058 | -0.25932 | | -4939.25293 | |
| | LS Fe(II) | -3 | -4939.42811 | -0.26216 | | -4939.25286 | |

**Table S7.** Computed DFT (TPSSh−D3/def2−TZVPP) energies of optimized hexa−coordinated FePPIX modes of Fe(*$OH^-$)($OH^-$). *Proximal axial ligand to the surface.

| Models | Oxidation and Spin states | *Q* | *E/def2-TZVPP*, hartree | *D3 correction*, hartree | $\Delta E_{(HS-LS)}$, kJ mol$^{-1}$ | *λ*, hartree | *λ*, kJ mol$^{-1}$ |
|---|---|---|---|---|---|---|---|
| **Free** | HS Fe(III) | -2 | -3250.47675 | -0.08594 | 82.4 | -3250.56933 | 47.1 |
| | HS Fe(II) | -3 | -3250.56764 | -0.08415 | 39.9 | -3250.45710 | |
| | LS Fe(III) | -2 | -3250.50815 | -0.08480 | | -3250.59463 | |
| | LS Fe(II) | -3 | -3250.58282 | -0.08484 | | -3250.50274 | |
| **Au 7 atoms** | HS Fe(III) | -2 | -4200.68789 | -0.17438 | 56.7 | -4200.80778 | 56.3 |
| | HS Fe(II) | -3 | -4200.76700 | -0.17204 | 193.8 | -4200.61067 | |
| | LS Fe(III) | -2 | -4200.70947 | -0.17187 | | -4200.82775 | |
| | LS Fe(II) | -3 | -4200.84081 | -0.17696 | | -4200.70109 | |
| **carbon** | HS Fe(III) | -2 | -4326.46198 | -0.18106 | 106.2 | -4326.57874 | 60.1 |
| | HS Fe(II) | -3 | -4326.57635 | -0.18373 | -4.2 | -4326.45659 | |
| | LS Fe(III) | -2 | -4326.50242 | -0.18181 | | -4326.59930 | |
| | LS Fe(II) | -3 | -4326.57475 | -0.17932 | | -4326.49901 | |
| **Au 13 atoms** | HS Fe(III) | -2 | -5015.26621 | -0.26217 | 53.5 | -5015.38047 | 73.5 |
| | HS Fe(II) | -3 | -5015.38821 | -0.25664 | 56.0 | -5015.24905 | |
| | LS Fe(III) | -2 | -5015.28659 | -0.25606 | | -5015.40010 | |
| | LS Fe(II) | -3 | -5015.40954 | -0.24950 | | -5015.26803 | |

**Table S8.** Computed DFT (TPSSh−D3/def2−TZVPP) energies of optimized hexa−coordinated FePPIX models with distal $OH_2$ and proximal $OH^-$, Fe(*$OH^-$)($OH_2$).

| Models | Oxidation and Spin states | *Q* | *E/def2-TZVPP*, hartree | *D3 correction*, hartree | $\Delta E_{(HS-LS)}$, kJ mol$^{-1}$ | *λ*, hartree | *λ*, kJ mol$^{-1}$ |
|---|---|---|---|---|---|---|---|
| **Free** | HS Fe(III) | -2 | -3250.97834 | -0.08862 | 44.5 | -3251.09392 | 73.1 |
| | HS Fe(II) | -3 | -3251.10544 | -0.08805 | -18.5 | -3250.97544 | |
| | LS Fe(III) | -2 | -3250.99528 | -0.08690 | | -3251.09743 | |
| | LS Fe(II) | -3 | -3251.09840 | -0.08674 | | -3250.98948 | |
| **Au 7 atoms** | HS Fe(III) | -2 | -4201.17730 | -0.17335 | 70.0 | -4201.31097 | 84.1 |
| | HS Fe(II) | -3 | -4201.29915 | -0.17304 | 42.7 | -4201.12346 | |
| | LS Fe(III) | -2 | -4201.20396 | -0.16938 | | -4201.31637 | |
| | LS Fe(II) | -3 | -4201.31543 | -0.18340 | | -4201.17099 | |
| **carbon** | HS Fe(III) | -2 | -4326.98749 | -0.18104 | 30.8 | -4327.09814 | 73.4 |
| | HS Fe(II) | -3 | -4327.08811 | -0.19034 | -2.8 | -4326.95827 | |
| | LS Fe(III) | -2 | -4326.99923 | -0.18194 | | -4327.10113 | |
| | LS Fe(II) | -3 | -4327.08706 | -0.18027 | | -4326.99401 | |
| **Au 13 atoms** | HS Fe(III) | -2 | -5015.74239 | -0.26720 | 51.3 | -5015.87784 | 85.5 |
| | HS Fe(II) | -3 | -5015.87382 | -0.26420 | 47.6 | -5015.72674 | |
| | LS Fe(III) | -2 | -5015.80454 | -0.26178 | | -5015.92453 | |
| | LS Fe(II) | -3 | -5015.89197 | -0.25305 | | -5015.73942 | |

**Table S9.** Computed DFT (TPSSh−D3/def2−TZVPP) energies of optimized hexa−coordinated FePPIX models with distal $OH^-$ and proximal $OH_2$, Fe(*$OH_2$)($OH^-$).

| Models | Oxidation and Spin states | *Q* | *E/def2-TZVPP*, hartree | *D3 correction*, hartree | $\Delta E_{(HS-LS)}$, kJ mol$^{-1}$ | *λ*, hartree | *λ*, kJ mol$^{-1}$ |
|---|---|---|---|---|---|---|---|
| **Au 7 atoms** | HS Fe(III) | -2 | -4201.16202 | -0.17222 | 46.3 | -4201.30081 | 104.6 |
| | HS Fe(II) | -3 | -4201.29040 | -0.17200 | 45.4 | -4201.11178 | |
| | LS Fe(III) | -2 | -4201.18091 | -0.16767 | | -4201.17409 | |
| | LS Fe(II) | -3 | -4201.30770 | -0.17093 | | -4201.17397 | |
| **carbon** | HS Fe(III) | -2 | -4326.97861 | -0.17390 | 74.1 | -4327.09277 | 84.5 |
| | HS Fe(II) | -3 | -4327.09391 | -0.17541 | 26.7 | -4326.97903 | |
| | LS Fe(III) | -2 | -4327.00684 | -0.17953 | | -4327.07516 | |
| | LS Fe(II) | -3 | -4327.10410 | -0.17813 | | -4327.00358 | |
| **Au 13 atoms** | HS Fe(III) | -2 | -5015.75310 | -0.27779 | 34.3 | -5015.88302 | 80.4 |
| | HS Fe(II) | -3 | -5015.87382 | -0.26767 | 104.3 | -5015.71290 | |
| | LS Fe(III) | -2 | -5015.76617 | -0.27546 | | -5015.89407 | |

**Table S10.** Reorganization Free Energies ($\lambda$, KJ mol$^{-1}$) of the Fe(III/II)PPIX Half Reactions Computed by DFT.

| $\lambda$, kJ mol$^{-1}$ | Free | Carbon | Au 13−atom |
|---|---|---|---|
| **−Fe (OH$^-$)** | 14 | 65 | 124 |
| **−Fe(*OH$^-$)(OH$^-$)** | 47 | 60 | 74 |
| **−Fe(*OH$_2$)(OH$^-$)** | 73 | 73 | 85 |
| **−Fe(*OH$^-$)(OH$_2$)** | − | 85 | 80 |

*The axial ligand proximal to the surface.

The reorganization energies in Table S9 do not correlate straightforwardly with the experimentally determined rate constants, Table 2. A "generic" rate constant form is thus[5, 6],

$$k_s = \kappa \frac{\omega_{eff}}{2\pi} \exp[-\frac{\lambda}{4k_B T}]$$

where $\omega_{eff}$ is the effective vibrational frequency of all the nuclear modes reorganized, $\kappa$ the electronic transmission coefficient, $k_B$ Boltzmann's constant, and $T$ the temperature. $\kappa << 1$ in the diabatic limit of weak electronic coupling between FePPIX and the electrode, while $\kappa \rightarrow 1$ in the opposite, adiabatic limit of strong interaction.

Most of the experimental rate constants are in the range 100~300 s$^{-1}$, i.e. with only a three−fold variation. The activation energy difference, i.e. the difference between $\lambda/4$ of the low−potential processes differs by only 2-5 kJ or a 2-8 fold rate constant difference in favor of carbon. The observed difference is in fact the opposite with $k_s$ of the low-potential process larger for gold than for carbon in spite of the larger computed value of $\lambda$. The observed differences are, however, too small that they can be estimated reliably by DFT.

The activation energy $\lambda/4$ for the same Fe(OH$^-$) species on carbon (low−potential) and gold (high−potential) is 15 kJ higher for the latter than for the former. This larger difference could be caused by a stronger contribution from reorganization of the gold surface itself than of the carbon electrode. The difference would give a 500-fold higher rate constant for carbon than for gold, but the observed values are in fact almost the same.

The apparent discrepancies could still be caused by a more favorable electronic transmission coefficient, i.e. stronger electronic interaction of FePPIX on gold than on carbon, as suggested by the DFT calculations. The former could then belong to the adiabatic limit and the latter to the (weakly) diabatic limit.

**Table S11.** Computed zero point energy (ZPE) in units of hartree, Gibbs free energy (G), and entropy (S) corrections in KJ $mol^{-1}$ and KJ $mol^{-1}$ $K^{-1}$ to each electronic state of free FePPIX with different axial ligands.

| Axial ligand | Oxidation and Spin state | *Q* | *ZPE*, hartree | *G*, kJ $mol^{-1}$ | *S*, kJ $mol^{-1}$ $K^{-1}$ |
|---|---|---|---|---|---|
| **−OH** | HS Fe(III) | -2 | 0.564546 | 1274.2 | 1.0357 |
| | HS Fe(II) | -3 | 0.562531 | 1263.1 | 1.0650 |
| | LS Fe(III) | -2 | 0.567396 | 1286.3 | 1.0104 |
| | LS Fe(II) | -3 | 0.564368 | 1270.4 | 1.0447 |
| **−(OH)(OH)** | HS Fe(III) | -3 | 0.575946 | 1291.5 | 1.1051 |
| | HS Fe(II) | -4 | 0.573497 | 1285.4 | 1.1011 |
| | LS Fe(III) | -3 | 0.578839 | 1297.1 | 1.1024 |
| | LS Fe(II) | -4 | 0.575491 | 1297.4 | 1.0693 |
| **−(OH)($OH_2$)** | HS Fe(III) | -2 | 0.588716 | 1324.5 | 1.1115 |
| | HS Fe(II) | -3 | 0.585914 | 1322.9 | 1.0805 |
| | LS Fe(III) | -2 | 0.591846 | 1341.7 | 1.0630 |
| | LS Fe(II) | -3 | 0.588057 | 1317.9 | 1.1263 |

**References**


(1) Sosna, M.; Fapyane, D.; Ferapontova, E. E. *J. Electroanal. Chem.* **2014**, *728*, 18-25.

(2) Guo, Y.; Deng, L.; Li, J.; Guo, S.; Wang, E.; Dong, S. *ACS Nano* **2011**, *5*, 1282-1290.

(3) Snyder, S. R.; White, H. S. *J. Phys. Chem.* **1995**, *99*, 5626-5632.

(4) Shigehara, K.; Anson, F. C. *J. Phys. Chem.* **1982**, *86*, 2776-2783.

(5) Kuznetsov, A. M.; Ulstrup, J. *Electrochim. Acta* **2000**, *45*, 2339-2361.

(6) Kuznetsov, A. M.; Ulstrup, J., Chapter 6 - The Simplest Chemical Process: Electron Transfer, pp 92-113; Chapter 7 - Some Selected Experimental Data for Simple Electron Transfer Reactions, pp 115-134. In: Electron Transfer in Chemistry and Biology. An Introduction to the Theory. *John Wiley & Sons, Chichester,* **1998**.